Embedded Based Quadratic Boost Converter with Sliding Mode Controller for the integration of Solar Photo-Voltaic source with Microgrid

Chitra Selvi. S, Ramya Govindaraj, Subrata Chowdhury, Saumya Singh, Baseem Khan

***Abstract*—A microgrid is a free-standing electrical network consisting of several energy sources and loads meant for specific applications or localized areas of operation. Power electronic converters are used in a microgrid for interfacing electrical sources and electrical loads of different power and voltage ratings with the standard bus bars of the microgrid. Microgrids use renewable energy sources like the wind and solar photo-voltaic energy source, and the fuel cell-based energy conversion systems. DC to DC converters is inevitable in a microgrid. The Quadratic Boost Converter (QBC) is a high voltage gain DC to DC converter with a single power electronic switch. In this work, the applicability of the Sliding Mode Controller (SMC) for the maximized harvest of energy from a solar photovoltaic system using the QBC is studied. Further, the capability of the QBC, along with an SMC, for the regulation of voltage across the terminals of the load, when the QBC acts as an interface between a load and the bus bar of the microgrid is also investigated. Relevant dynamic equations are derived from fundamental principles. The proposed model is simulated in the MATLAB/Simulink environment and experimentally verified.**

***Index Terms*— Microgrid, Quadratic Boost Converter, Microcontroller, Maximum Power Point Tracking**

I. INTRODUCTION

MICROGRID systems with standardized operational features and protocols are coming up recently [1]. Where human habitats are not connected to the national grid an AC or DC microgrid can be used. Microgrids of DC or AC or hybrid AC DC types are applicable for industrial establishments like manufacturing or processing plants. A microgrid consists of several AC or DC sources, loads and bus bars. A microgrid may include one or more bus bars operating with different voltages and may be AC or DC [2]. The voltage ratings of the bus bars and the type of the bus bars to be used in a microgrid are selected according to the applications including the different loads and the different electrical sources to be connected to the microgrid.

CSelvi. S is with Department of EEE in University College of Engineering, Dindigul, Tamilnadu, India (e-mail: chitraselvi2020@gmail.com).

RGovindarajis with School of Information And Technology, VIT Vellore, India (e-mail: ramyag@vit.ac.in).

S Chowdhury is with department of Computer Science and Engineering, Sreenivasa Institute of Technology and Management Studies, India (e-mail: subrata895@gmail.com).

S Singh is with EED, IIT (BHU) Varanasi, India (e-mail: saumyasingh.rs.eee20@itbhu.ac.in).

B Khan is with Department of Electrical and Computer Engineering, Hawassa University, Hawassa, Ethiopia, (e-mail: baseem.khan04@gmail.com).

DC to DC converters like the generic buck, boost, and buck-boost converters are popular for a long time and they are basic units of power electronic conversion systems. Numerous novel power electronic converter topologies have also been derived from the DC to DC converters.

While the buck DC to DC converter exhibits a linear correlation among the controlled variable (Output Voltage) and the manipulated variable (Duty Cycle), the other two basic converters like the boost or the buck-boost converter exhibit a non-linear relationship [3]. When a large voltage gain is required a large duty cycle is required. The characteristics relating duty cycle and voltage gain of the boost or the buck-boost converters are highly non-linear and it becomes difficult to design traditional controllers like the Proportional and Integral converters [4].

The SEPIC, CUK and LUO converters are the smatter of DC to DC converters [5][6][7]. These developed converters guarantee better source side and load side power quality characteristics like minimization of ripple. The SEPIC, the CUK, and the Positive output LUO converters are buck-boost converters with the same voltage gain given by the voltage gain equation,

$$\text{Voltage Gain} = D/(1-D) \quad (1)$$

where D is the duty cycle. The number of components used in DC to DC converters is almost the same. Using the same number of components, the different topologies like the SEPIC, CUK and the LUO converters are formed. Since all these converters use a set of two inductors and two capacitors the transfer function among the duty cycle and the output voltage for all these converters is of order four [8].

The QBC on the other hand also uses the same number of components with just two more diodes and offers quadratic high voltage gain. The QBC can be visualized as the cascading of two generic boost converters [9]. A generic boost converter uses a single power electronic switch, a single diode, a single inductor, and a single capacitor. Since the QBC can be visualized as the cascade of two generic boost converters the order of the transfer function of the QBC is four.

Almost all DC to DC converters exhibits a non-linear relationship between the controlled parameter and the manipulated parameter. The Proportional, Integral and differential (PID) [10] controllers, the fuzzy logic controllers (FLC) [11], the Artificial Neural Network (ANN) [12] based controllers, the ANFIS [13] controllers, the internal model controllers (IMC) [14] all have been proposed and validated by many researchers.

Further, when the interface between the load or a battery or a DC voltage bus bar and the Solar Photo Voltaic (SPV) energy harvesting system the DC to DC converters work with the focus of harvesting the ultimate power for the given environmental conditions [15]. Maximum Power Point Tracking (MPPT) is incorporated in the DC to DC converters which draw power from the solar PV panels and deliver power to the load.

There are techniques for achieving MPPT when harvesting power from renewable sources like the SPV or the WECS. With SPV sources the popular MPPT techniques [16] and the Incremental Conductance (INC) [17] technique. These techniques require the measurement of the terminal voltage of the SPV source and the current supplied by the SPV source.

The Sliding mode Controller is a relatively novel method of controller that has been adopted for the MPPT of SPV sources. In [18] the authors have used a buck converter along with the MPPT scheme for the harvest of the solar power source.

In this work, the performance of the SMC with the QBC as a boost converter is analyzed from the perspective of the output voltage regulation. The performance of the SMC has been compared with other popular techniques like the PI controller and the Fuzzy Logic controllers. The performance of the SMC with the QBC has also been analyzed from the perspective of an MPPT controller.

The State Space analysis of electrical networks gives a deeper insight into the dynamics of the networks [19]. The Power electronic circuits, since they contain semiconductor switches that are discretely switched the power electronic circuit can be treated as a set of two linear electrical circuits being active for two different periods dictated by the ON and OFF periods of the duty cycle. Therefore, the average state-space analysis has become a standard practice for the study of the power electronic circuits [20]

The basic dynamic equations in the state space form of the QBC have been derived and the simulations in the MATLAB SIMULINK environment have been studied. A circuit model with the different control schemes has also been studied. The performance of the SMC as an MPPT controller for the QBC has also been developed and validated. Experimental verifications with a suitable prototype have also been carried out and finally, it has been established that the QBC with SMC is a better candidate as a voltage regulation unit when fed from standard DC sources and also a good MPPT system can be built around the QBC with the SMC.

The contents of the rest of the paper are arranged as follows. Next to this introduction, the topology of the QBC is presented and the State Space modeling is carried out in the second section. Open-loop studies using the State Space model, by way of simulations in the MATLAB environment have been presented in this section. The discussions on building an SMC based MPPT scheme using the QBC is presented in the third section. The development of an output voltage regulation of a QBC with SMC and its performance in the face of disturbances on the source and the load sides are presented in the fourth section. The details of the experimental verification are given in the fifth section. A discussion on the comparison of results obtained in simulations and experimental verifications are carried out in the sixth section followed by the conclusion.

II. A Quadratic Boost Converter Topology and the State Space Model

The QBC is a DC to DC converter with a high voltage gain. As compared to the basic or Generic Boost Converter (GBC) for which the voltage gain is expressed in eq. (2) the gain voltage of the QBC is quadratic and is expressed in eq. (3).

$$V_{out} = {V_{in}}/{1 - d} \quad (2)$$

$$V_{out} = {V_{in}}/{(1 - d)^2} \quad (3)$$

The relationship between the steady-state gain voltage of the GBC and the QBC is given in figures 1 and 2.

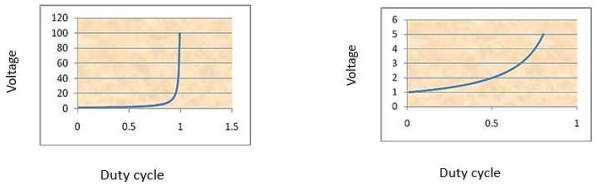

(a) (b)

Figure 1. The Voltage Gain characteristics of the GBC, (a) D in the range of 0.0 to 1.0, (b) D in the range of 0.0 to 0.8

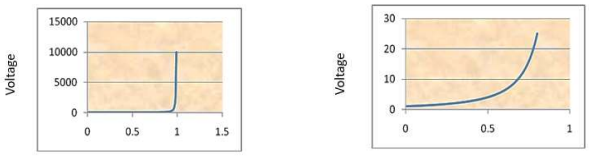

(a) (b)

Figure 2. The Voltage Gain characteristics of the QBC, (a) D in the range of 0.0 to 1.0, (b) D in the range of 0.0 to 0.8

Concerning Figures 1 and 2, the gain voltage of the QBC is immense than the GBC.

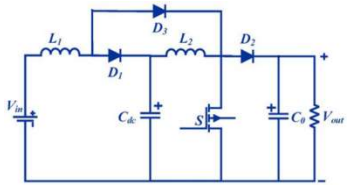

Figure 3. Topology of the QBC

The topology of the QBC is given in figure 3. Four storage elements comprise of two inductors and two capacitors. In addition to the main power electronic switch, three diodes are also used. A large number of storage elements increase the order of the system and a large number of power electronic semiconductors there are chances of higher switching losses. In spite of these drawbacks, the QBC has gained popularity because of the straight forward operational features and the easy controllability offered by the QBC.

III. Operational Mechanism of the QBC

The operational mechanism of the QBC can be studied by considering the structure or topology of the QBC. Regarding figure 3 the topology of the QBC suggests that the QBC is nothing but a set of two GBC units cascaded in series. The first unit consists of inductor L_1, diode D_1, and capacitor C_1. The second GBC consists of the second inductor L_2, the

second diode D_2, and the capacitor C_2. The second GBC unit has a power electronic switch S and the first GBC unit does not have its power electronic switch.

As per the figure 3, a set of two GBCs can be cascaded with two sets of inductors, diodes, and switches. In the cascaded GBCs the switches S_1 and S_2 may be operated simultaneously. Essentially, in the QBC the switch S is shared by both the first and the second GBC units. The diode D_3 facilitates the direct use of the common switch S by the first GBC unit while it prevents the backflow of power from the aspect of output to the input hand which are similar to the action of the other two diodes D_1 and D_2.

The first GBC output appears across the capacitor C_1. The voltage astride the capacitor C_1 is the input to the second stage. If V_{in} is the input voltage, then the output of the first stage can be given as

$$V_{out1} = V_{in1}/1 - D \quad (4)$$

For the second stage, the input is V_{out1}, therefore, the output of the second stage will be as shown in equation (5).

$$V_{out2} = (V_{out1}/1 - D) \quad (5)$$

The two equations (4) and (5) can be combined as shown in equation (6).

$$V_{out\,2} = \left(\frac{(V_{in1}/1-D)}{1-D}\right) = \frac{V_{in1}}{1/(1-D)^2} \quad (6)$$

The circuit model simulation in the MATLAB/Simulink shows the following results that validate this discussion. Fig. 4 shows the source side voltage. Fig. 5 shows the step-change in duty cycle. Fig. 6 shows the Response of the output voltage.

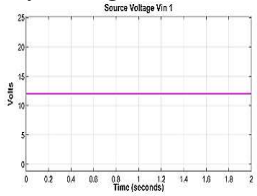

Figure 4 Source side voltage 12 V

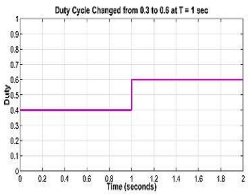

Figure 5 step-change in duty cycle

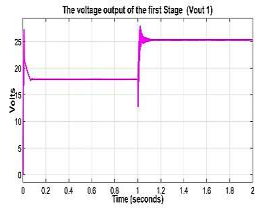

(a)

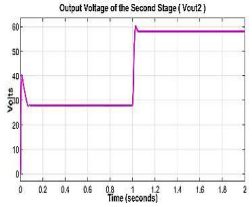

(b)

Figure.6. Response of the output voltage, (a) step-change in duty cycle for GBC, (b) step-change in duty cycle for QBC

Regarding the results of the simulations carried out in MATLAB/Simulink, it can be confirmed that the output of the first and the second stages for a duty cycle of 0.4 are respectively around 17.9 V and 27.94 V. The following calculations hold good.

$$V_{out\,1} = V_{in\,1} * (1/(1-D)) = 18 \text{ V} \quad (7)$$

$$V_{out\,2} = V_{in\,2} * (1/(1-D)) = 30 \text{ V} \quad (8)$$

In the simulations the exact values for $V_{out\,1}$ and $V_{out\,2}$ are respectively 17.9V and 27.94V and the difference between the calculated values and the simulated values can be attributed to the forward voltage drops of the MOSFET and the diodes D_1, D_2 and D_3. Similarly, regarding the results of the simulations carried out in MATLAB/Simulink it can be confirmed that the output of the first and the second stages for a duty cycle of 0.6 are respectively around 25.32 V and 58.15 V. The following calculations hold good.

$$V_{out\,1} = V_{in\,1} * (1/(1-D)) = 30 \text{ V} \quad (9)$$

$$V_{out\,2} = V_{in\,2} * (1/(1-D)) = 70 \text{ V} \quad (10)$$

In the simulations, the exact values for $V_{out\,1}$ and $V_{out\,2}$ are respectively 25.329V and 58.15V and the difference between the calculated values and simulated values can be attributed to the forward voltage drops of the MOSFET and the diodes D_1, D_2 and D_3. It is to be noted that the drop of voltage in the first stage causes a huge difference between calculated values and the simulated values for the second stage.

IV. Derivation of the Voltage Gain from Fundamental Principles

Although the voltage gain obtained from the earlier discussion it is evaluated using simulations in the MATLAB/Simulink the voltage gain of the QBC can be derived from the first principles as discussed in this section.

The topology of QBC is shown in figure 3. There is a common switch S, which changes the circuit into two different modes. Mode 1 is obtained when the status of switch S is ON and Mode 2 is obtained when the status of switch S is OFF. The two structures of Mode 1 and 2 are shown in figures 7 and 8. By applying Kirchhoff's voltage law, the basic voltage equations of two modes of operation can be formed.

Regarding figure 7, of Mode 1 the voltage source is connected across Inductor L_1. According to the Kirchhoff's voltage law for Mode 1, for a period D, $V_{L1}(D) = V_s$ and $V_{L2}(D) = V_{C1}$; Similarly, for the mode 2 configuration as shown in figure 8 the voltage equations are $V_{L1}(1\text{-}D) = (V_s - V_{C1})(1\text{-}D)$ and $V_{L2}(1\text{-}D) = ((V_{C1} - V_0)(1\text{-}D)$. When a duty cycle of D is used mode 1 is operational for a period D and mode 2 for a period 1 – D. To maintain the voltage drop across an inductor is zero over a switching cycle. This implies that the following condition should be satisfied.

$$D\,(V_{L1}(D)) + (1\text{-}D)\,V_{L1}(1\text{-}D) = 0 \quad (11)$$

$$D\,(V_s) + (1\text{-}D)\,(V_s - V_{C1}) = 0$$

$$DV_s + V_s - DV_s - V_{C1} + DV_{C1} = 0$$

$$V_{C1}/V_s = 1/(1\text{-}D)$$

Similarly, the voltage balance of inductor 2 is as follows

$$D\,(V_{L2}(D)) + (1\text{-}D)\,V_{L2}(1\text{-}D) = 0 \quad (12)$$

$$D\,(V_{C1}) + (1\text{-}D)\,(V_{C1} - V_0) = 0$$

$$DV_{C1} + V_{C1} - V_0 - DV_{C1} + DV_0 = 0$$

Since $V_{C1}/V_s = 1/(1\text{-}D)$ and Substituting $V_{C1} = V_s/(1\text{-}D)$

$$D(V_s/(1\text{-}D) + V_s/(1\text{-}D) - V_0 - D\,(V_s/(1\text{-}D) + DV_0 = 0$$

Multiplying the whole by (1-D),

$$DV_s + V_s - V_0(1\text{-}D) - DV_s + D(1\text{-}D)\,V_0 = 0$$

$$DV_s + V_s - V_0 + DV_0 - DV_s + DV_0 - D2V_0$$

$$V_s = V_0 - 2DV_0 + D2V_0$$

$$V_s = V_0\,(D^2 + 1 - 2D)$$

$$V_0/V_s = 1/\,(D^2 + 1 - 2D) = 1/(1\text{-}D)^2$$

4.1. The State Space averaged model of the QBC

The state-space average modelling is an important procedure to get an insight into the dynamics of the system for the given circuit parameters like source voltage, the load and the other circuit components connected in the topology.

Besides, power electronic converters are variable structure systems and they usually work in different structures depending upon the switching states of the power electronic

switches involved. In the case of the QBC, there is only one power electronic switch.

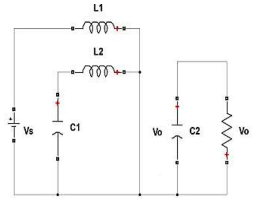

Figure 7. Mode 1operation

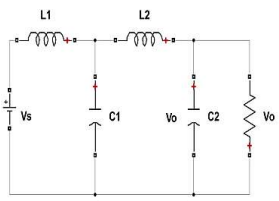

Figure 8. Mode 2 operation

The switch is ON for a period D and OFF for a period, 1–D. Based on the two positions of the switch, two modes of operation are considered. During each mode of operation, the topology is differently configured. The diodes which are forward biased are considered as closed-circuit elements and those diodes that are reverse biased are considered as open circuit elements. The two topological substructures are considered for the two different durations of D and (1-D) within one switching cycle. During these two periods, the substructures formed are considered linear and separate state equations are drawn out. Then depending upon the periods D and (1-D) an average model is formed by the application of the following procedure.

$dX/dt = A_1 * X + B_1 * Y$ for the period D

$dX/dt = A_2 * X + B_2 * Y$ for the period (1-D)

The final $dX/dt = (A_1*D)*X + (A_2*(1-D))\ X + (B_1*D)*Y + (B_2(1-D))*Y$

In the proposed QBC for the given circuit parameters as shown in Table 1, the state-space averaged model has been produced and the associated simulation results are given.

Table 1. Circuit Parameters

Parameter	Value	Unit
Nominal Source Voltage	12	Volts
Inductor L_1	1.00	Milli Henry
Inductor L_2	1.00	Milli Henry
Capacitor C_1	2200	Micro Farad
Capacitor C_2	2200	Micro Farad
Load resistance	48	Ohms
Nominal Power Output	48	Watts

During switching period D, concerning figure 7 the following equations are obtained.

$$V_{in1} = (L_1 * \frac{\mathrm{di_{L1}}}{\mathrm{dt}}), V_{C1} = (L_2 * \frac{\mathrm{di_{L2}}}{\mathrm{dt}})$$

$$\frac{\mathrm{dV_{C1}}}{\mathrm{dt}} = \mathrm{i_{L2}}/\mathrm{C_1}, \frac{\mathrm{dV_{C2}}}{\mathrm{dt}} = {}^{\mathrm{V_{C2}}}/_{\mathrm{R_{C2}}} \qquad (13)$$

During switching period 1-D, concerning figure 8 the following equations could be obtained.

$$V_{in1} = \left(L_1 * \frac{di_{L1}}{dt}\right) + V_{C1}$$

$$V_{C1} - V_{C2} = (L_2 * {}^{\mathrm{di_{L2}}}/_{\mathrm{dt}})$$

$$\frac{\mathrm{dV_{C1}}}{\mathrm{dt}} = (\mathrm{i_{L1}} - \mathrm{i_{L2}})/\mathrm{C_1}$$

$$\frac{\mathrm{dV_{C2}}}{\mathrm{dt}} = (\mathrm{i_{L2}}/\mathrm{C_2}) - \frac{\mathrm{V_{C2}}}{\mathrm{RC_2}} \qquad (14)$$

The state-space model of the system during period D is given in equation (15). The state-space model of the system during period 1 – D is given in equation (16). By employing the principle of finding the average state matrix as $A = D*A_1 + (1-D) * A_2$ and the average input matrix $B = D* B_1 + (1-D)*B_2$, the state equation of the state space averaged model is given in equation (17).

$$\begin{bmatrix} \frac{di_{L1}}{dt} \\ \frac{di_{L2}}{dt} \\ \frac{dv_{C1}}{dt} \\ \frac{dv_{C2}}{dt} \end{bmatrix} = \begin{bmatrix} 0 & 0 & 0 & 0 \\ 0 & 0 & \frac{1}{L_2} & 0 \\ 0 & \frac{-1}{C_1} & 0 & 0 \\ 0 & 0 & 0 & \frac{-1}{RC_2} \end{bmatrix} * \begin{bmatrix} i_{L1} \\ i_{L2} \\ v_{C1} \\ v_{C2} \end{bmatrix} + \begin{bmatrix} \frac{1}{L_1} \\ 0 \\ 0 \\ 0 \end{bmatrix} * V_{in1} \qquad (15)$$

$$\begin{bmatrix} \frac{di_{L1}}{dt} \\ \frac{di_{L2}}{dt} \\ \frac{dv_{C1}}{dt} \\ \frac{dv_{C2}}{dt} \end{bmatrix} = \begin{bmatrix} 0 & 0 & \frac{-1}{L_1} & 0 \\ 0 & 0 & \frac{1}{L_2} & \frac{-1}{L_2} \\ \frac{1}{C_1} & \frac{-1}{C_1} & 0 & 0 \\ 0 & \frac{1}{C_2} & 0 & \frac{-1}{RC_2} \end{bmatrix} * \begin{bmatrix} i_{L1} \\ i_{L2} \\ v_{C1} \\ v_{C2} \end{bmatrix} + \begin{bmatrix} \frac{1}{L_1} \\ 0 \\ 0 \\ 0 \end{bmatrix} * V_{in} \qquad (16)$$

$$\begin{bmatrix} \frac{di_{L1}}{dt} \\ \frac{di_{L2}}{dt} \\ \frac{dv_{C1}}{dt} \\ \frac{dv_{C2}}{dt} \end{bmatrix} = \begin{bmatrix} 0 & 0 & \frac{D-1}{L_1} & 0 \\ 0 & 0 & \frac{1}{L_2} & \frac{D-1}{L_2} \\ \frac{1-D}{C_1} & \frac{-1}{C_1} & 0 & 0 \\ 0 & \frac{1-D}{C_2} & 0 & \frac{-1}{RC_2} \end{bmatrix} * \begin{bmatrix} i_{L1} \\ i_{L2} \\ v_{C1} \\ v_{C2} \end{bmatrix} + \begin{bmatrix} \frac{1}{L_1} \\ 0 \\ 0 \\ 0 \end{bmatrix} * V_{in} \qquad (17)$$

The averaged State Space Model is simulated in the MATLAB/Simulink environment is given in figure 9.

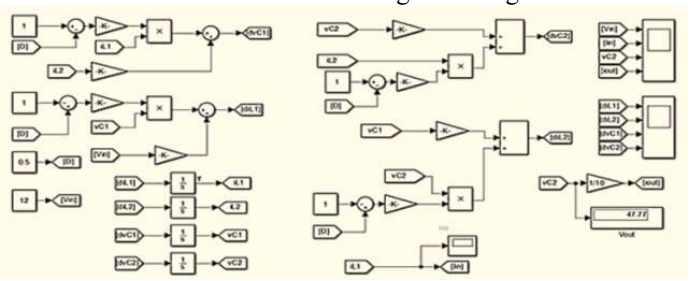

Figure .9. Implementation of Averaged State Space Model of the QBC

The results obtained in the simulation of the averaged state-space model in MATLAB are as shown in figures 10 to 12.

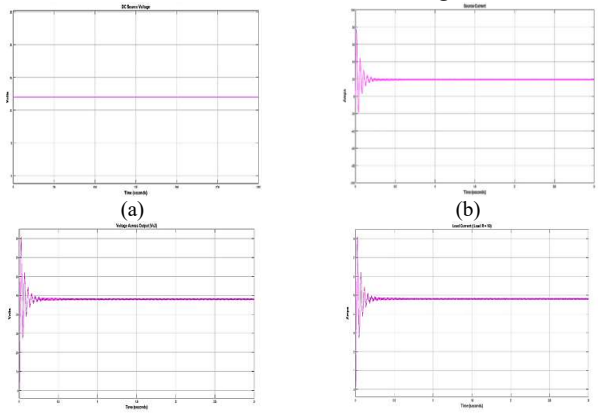

(a) (b) (c) (d)

Figure 10. source Voltage and current variations, (a) The source voltage Vin = 12 V (b) The Source Current with a duty cycle of 0.5 and load R = 10 Ohms (c) The Voltage Across the load (Output voltage) (d) The load current with load R = 10 Ohms and output voltage = 48 V with D= 0.5

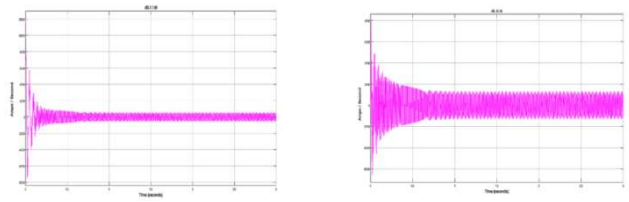

(a) (b)

Figure 11.The change of the current rate through inductors
(a) The change of the current rate through inductor L_1. (b) The change of the current rate through inductor L_2

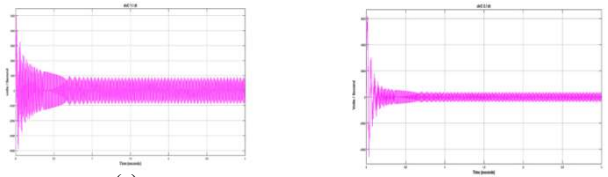

(a) (b)

Figure 12. Change of the voltage across capacitors (a) Change of the voltage rate across capacitor C_1. (b) Change of voltage rate across Capacitor C_2

4.2 Circuit Model of the QBC

Fig. 13 shows the circuit model of QBC.

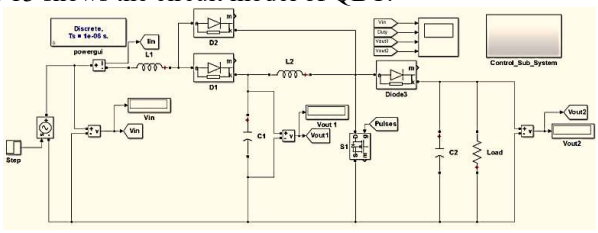

Figure 13. Circuit model of the QBC

Fig. 14(a) shows the voltage source at 12 V. Fig. 14(b) shows a step-change in the duty cycle. Fig. 14(c) presents the reaction of the output for the change in the duty cycle.

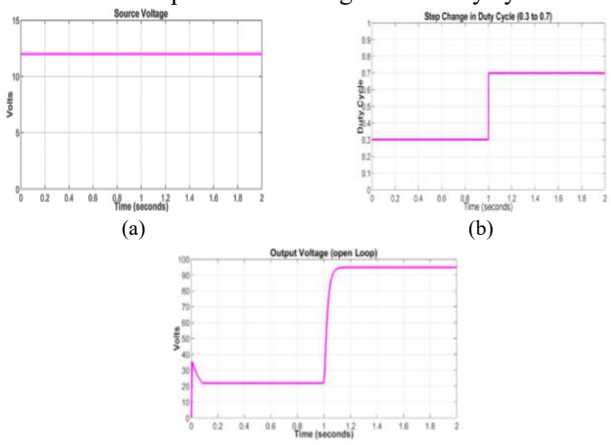

(a) (b)

(c)

Figure 14. (a) The voltage source at 12 V (b) A step-change in the duty cycle (c) The reaction of the output for the change in the duty cycle

4.3. SMC of QBC and Lyapunov stability analysis

Fig. 15 shows the simulink model of the SMC for the QBC.

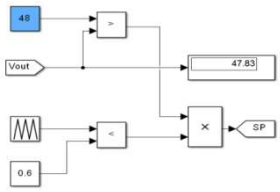

Figure 15. The SIMULINK realization of the SMC for the QBC

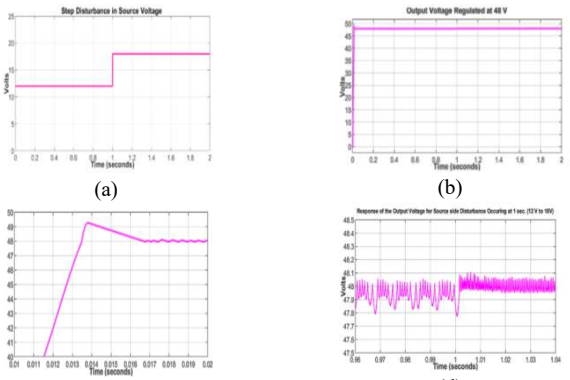

(a) (b)

(c) (d)

Figure 16. (a) Step disturbance in the source voltage from 12 V to 18 V, (b) Regulation of the output voltage at 48 V, (c) Peak overshoot (d) There is no significant overshoot if the system encounters a source side disturbance

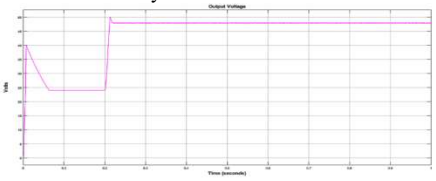

Figure 17. Response of the SMC with a change of command

Fig. 16 (a) shows the step disturbance in the source voltage from 12 V to 18 V. Fig. 16(b) shows the regulation of the output voltage at 48 V. Fig. 16(c) shows the peak overshoot and fig. 16(d) shows that there is no significant overshoot if the system encounters a source side disturbance. Fig. 17 shows the response of the SMC with a change of command from 24 V to 48 V at 1 sec. Table 2 shows the performance of the Sliding Mode Controller.

Table 2 Performance of the Sliding Mode Controller (SMC)

Controller	Peak Overshoot	Transient Period	Steady State Error
SMC	2.2 V	18 ms	0.4 V

4.4 Implementation of a PI controller for the QBC

The PI controller is a popular general-purpose controller suitable for regulatory operations. In the context of the QBC, it may be needed to improve the output voltage of the QBC at the desired level irrespective of the disturbance that could occur on the source side voltage or the disturbances caused in the load side.

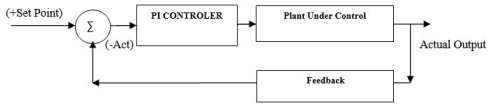

Figure.18. Block diagram of the PI controller implementation

The Block diagram of a closed-loop controller using the PI controller is shown in figure 18.

Regarding the block diagram shown in figure 18, the whole system contains the plant under control, a feedback system, the summing unit, and the PI controller. The parameter to be controlled is measured and supplied to the feedback subsystem. The feedback subsystem may introduce either attenuation or an amplification depending upon the scaling used for the command input derived out of the plant.

4.5 Tuning of the PI controller

For the required performance of the PI controller, it has to be tuned appropriately. The most popular method of tuning the PI controller is by the Zeigler Nicholas (ZN) technique. There are

two methods of tuning the PI controller by the ZN technique. The first method is the reaction curve method.

For the QBC under consideration, the reaction curve is drawn by giving a step input of the duty cycle of 0.5. The reaction curve obtained is shown in figure 19.

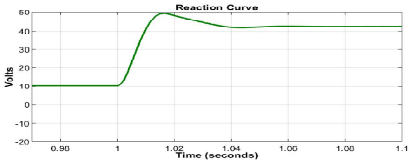

Figure 19. The reaction curve when a step input is applied

By the simple procedure following the ZN technique, the K_p and K_I values are represented in table 3.

Table 3 K_p and K_I values of the PI controller

K_p	0.25
K_I	0.5

Figure 20 shows the response of the PI controller with the command changed from 24 V to 48 V at time instant 1 second. The overshoot while at startup when the command is 24 V is more as compared to the overshoot when the command is 48 V. The average steady-state error is found to be nearly 0.8 V and the ripple at the output voltage is 1.6 V Peak to peak. Table 4 shows the performance of the PI controller.

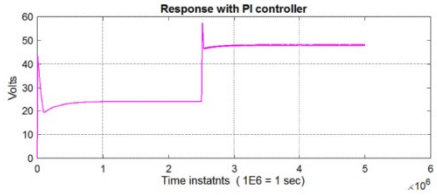

Figure 20. The response of the PI controller

Table 4 Performance of the PI controller

Controller	Peak Overshoot	Transient Period	Steady State Error
PI	10 V	200 Micro Sec	0.8 V

4.6. Implementation of Fuzzy Logic Controller for QBC

A fuzzy logic controller (FLC) is a control scheme based on the fuzzy algebra. The FLC belongs to the category of intelligent controllers. The decision making uses the human experience which is imparted to the control system in the form of simple rules. The FLC, unlike the Artificial Neural Network, cannot learn by itself but it can use third party experience in the form of a knowledge base. The knowledge base supplied to the FLC is usually in the form of a lookup table 5 consisting of a certain number of 'IF-THEN ' rules.

FLC can be used under different circumstances and mainly they are used when there is no mathematical model available for the system to be controlled or that the available mathematical model is either complex or highly nonlinear.

In the context of the QBC, the open-loop characteristics of the QBC relating the output voltage V_{out} and the duty cycles are highly nonlinear and hence we can opt for the FLC. The FLC is intelligent and is adaptive as well.

4.7. Methodology of the FLC

In the context, output voltage regulation of the QBC two variables are supplied to the front end of the FLC. These two are the setpoint (SP) voltage and the actual (Act) voltage. The difference between these two is called the error. The difference between the present error or the current error (CE) and the error observed in the previous measurement (PE) is called the change in error.

Thus, the current error (CE) = SP – Act (Current Value);

The past error (PE) = SP – Act (Actual Value measured in the previous cycle)

The change in error = PE – CE = ∂E;

The two terms namely the CE and ∂E are then normalized on a universal scale that ranges typically between -100 and +100 or -1 and +1. The following terminology associated with the Fuzzy Logic Control system is important.

Universe of Discourse (UOD): The complete range of the variable under consideration. It could be the output parameter, the manipulated parameter like the duty cycle, the error.

Segmentation: UOD of the given parameter is divided into some segments. Each segment is assigned with a meaningful name. The names of the segments are called the linguistic variables. Unlike the conventional variables like x, y or z used in algebra the linguistic variables have some relevant meaning.

Normalization: If many variables are associated in a process control systems then the actual full range of the individual variables are to be converted into a common scale like the Per Unit scale or the percentage scale. This operation is called Normalization. After normalization, all the variables involved in the process control are transformed to the common scale.

Fuzzification: It is the process in which the degree of the given variable in a given segment of the UOD is found. The extent of membership of a variable in a particular segment is a function of the normalized value of the variable and the membership function. The membership function is a curve o some specified shape drawn over the segment and the shape of the membership function differs from problem to problem.

Fuzzy Engine: It is the system that implements the fuzzy logic control algorithm. The Fuzzy engine carries out its job in two phases. In the first phase, considering the membership function of the inputs to the fuzzy engine the segment in which the output lies is first found out. In the second phase, the exact value of the output to be implemented is found out. Finally, the output in the fuzzified form is defuzzified using any standard defuzzification method like the centroid method.

In a typical regulatory control system like the output voltage regulation of the QBC, the error and the change in error is first found as shown in figure 21 (a), and then these two are fuzzified. After fuzzification, a rule matrix as shown in figure 21(b) is used to locate the segment in which the manipulated variable should lie in its UOD.

MATLAB provides a convenient toll box for implementing Fuzzy logic control. Figures 21 (a), 21(b), and 21(c) show the important screenshots of MATLAB associated with the FLC.

The response of the FLC controlled QBC is shown in figure 21(c). The parameters of the QBC used remain the same for the results of FLC as shown in table 6.

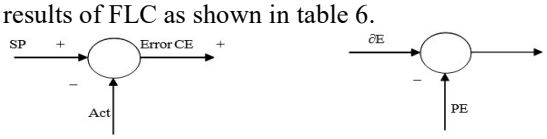

Figure 21(a). The estimation of Error and Change in Error

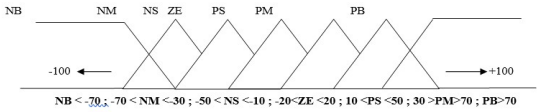

Figure 21 (b). The Triangular Membership Functions

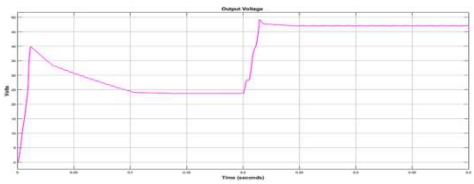

Figure 21 (c). The response of output voltage with FLC

4.8. The Integral Square Error

The Integral Square Error (ISE) is a measure of performance index of regulatory controllers like the PI controller (in figure 22(a)) or Fuzzy Logic Controller or SMC controller (in figure 22(b)).

Table 5: Rules

	Error							
		NB	NM	NS	ZE	PS	PM	PB
Change in error	NB	NB	NB	NM	NM	NS	NS	ZE
	NM	NB	NM	NM	NS	NS	ZE	PS
	NS	NM	NM	NS	NS	ZE	PS	PS
	ZE	NM	NS	NS	ZE	PS	PS	PM
	PS	NS	NS	ZE	PS	PS	PM	PM
	PM	NS	ZE	PS	PS	PM	PM	PB
	PB	ZE	PS	PS	PM	PM	PB	PB

Negative Big (NB), Negative Medium (NM), negative Small (NS), Zero (ZE), Positive Big (PB), Positive Medium (PM) and Positive Small (PS)

Table 6. The results of FLC

Controller	Peak Overshoot	Transient Period	Steady State Error
FLC	1.2 V	15 ms	0.8V

The estimation of the ISE involves the integration of the squares of the instantaneous values of errors. The ISE is estimated over the period commencing from the instant of a new command or a change in the source voltage or load current until the system reaches the steady-state value.

The ISE is a comprehensive measure of performance that takes into consideration the peak overshoot, the oscillations, the transient period and the steady-state error, as shown in figure 22(c).

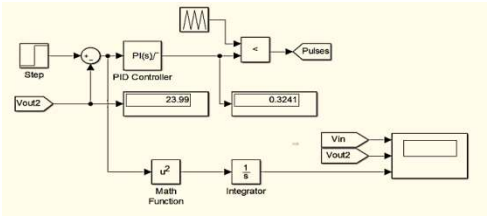

Figure 22(a). PI controller with a provision to read ISE

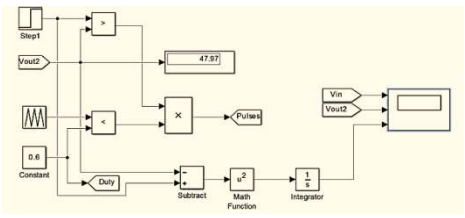

Figure 22(b). Implementation of SMC with provision to measure ISE

In this work, the performance of the PI controller and the FLC are compared for identical conditions of operations. The results of simulations reveal that the performance of the SMC is better than the PI controller and the Fuzzy Logic Controller, as shown in table 7. With the Fuzzy Logic controller, the system is adaptive and it is easier to design since it does not require a mathematical model.

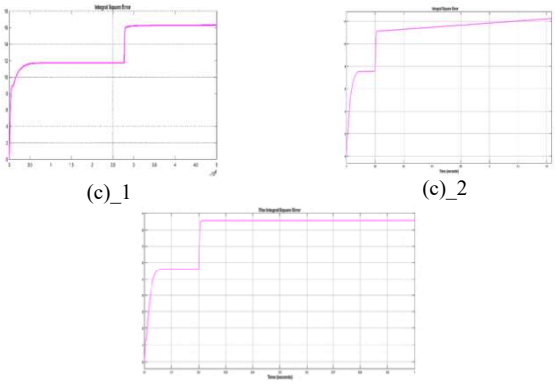

(c)_1 (c)_2 (c)_3

Figure 22(c): (1) The integral square error with PI controller, (2) Integral square error with FLC, (3) Integral Square Error with SMC

Table 7: Comparative analysis of utilized controllers

Controller	Peak Overshoot	Transient Period (ms)	Steady State Error	Integral Square Error	Ripple at Output DC
PI	10 V	200 ms	0.8 V	16.4	0.2 V
FLC	1.2 V	15 ms	0.8V	12.2	0.8V
SMC	2.2 V	18 ms	0.4 V	8.6	1.3 V

The PI controller is difficult to design tune and implement. However, in the DC output voltage the presence ripple content is the least in the PI controller.

V. The Experimental Verifications

An experimental verification prototype has been built to evaluate the proposed idea of the QBC to be driven by the SMC. For the experimental verifications, the specifications were the same as used for the simulations and are shown in table 8. Figure 23 shows the experimental set up of the proposed research.

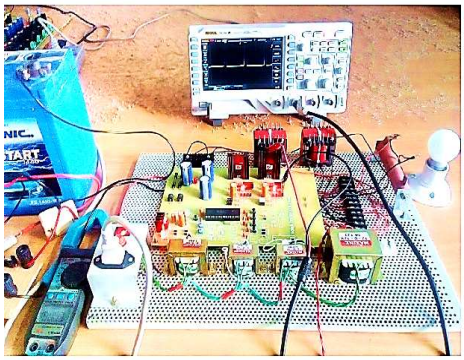

Figure 23. Photograph of the experimental Prototype

Table 8. Experimental parameters

Nominal Power Rating	50W
Nominal Input Voltage	12V DC
Nominal Output Voltage	48 V DC
Load	50 Ohms resistor
Power Electronics Switch	IRF 540
Inductors L1=L2	1 mH

Capacitor C1=C2	2200 MFD
Switching Frequency	5 kHz
Microcontroller	PIC 16F877A
Isolation Optocoupler	MCT2E

The closed-loop controller was implemented using the Analog inputs available in the microcontroller. A 0-5 DC voltage was used to set the desired voltage with a scaling of 4.8 V corresponding to 48 V. The actual output voltage was attenuated using a resistive network and the scaling factor was used.

The PWM 1 channel is available with the microcontroller at pin no 17 was used to deliver the switching pulses to the Optocoupler. The important waveforms obtained using the experimental setups are shown in the figures from 24 to 25. Figure 24(a) gives the switching pulse with a duty cycle of 0.5. The durations one switching cycle was 200 milliseconds and the ON and OFF timings are respectively 99 milliseconds and 101 milliseconds.

Regarding figure 24(b) the source voltage was disturbed from 12 V to v10 V and then to 12 V at different time instants and the output voltage was observed to stay at 48 V. The controller adopted was the SMC and the output exhibits less chattering at a lower input voltage of 10 V and the more chattering when the source voltage was 12 V.

When the SMC is in action two different duty cycles of 0.6 and 0.1 were used alternately when the output voltage deviated from the desired value of 48V. With the actual output voltage crossing the 48 V level and going up the duty cycle was changed from 0.6 to 0.1 and as the output voltage falls below the 48V the duty cycle was changed from 0.1 to 0.6. The resulting square pulses as applied to the Optocoupler is represented in figure 24(c).

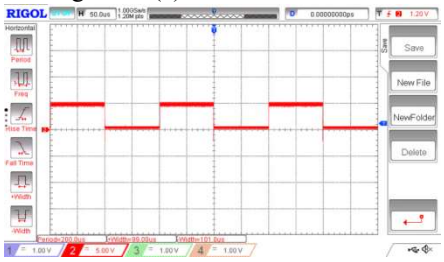

Figure 24(a).The switching pulses duty cycle close to 0.5

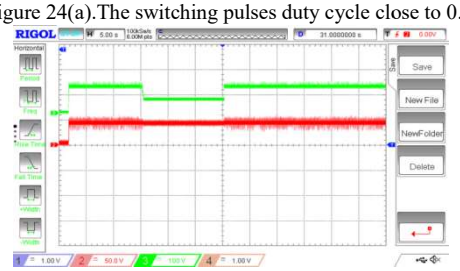

Figure24(b).Output voltage regulated at 48 V with source disturbed from 12 V to 10 V to 12V.

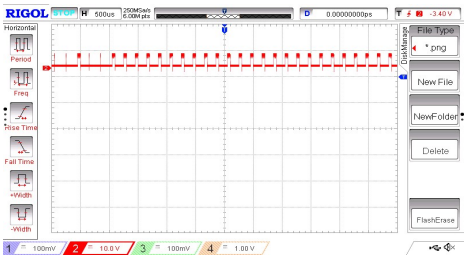

Figure.24(c). The switching pulses applied to the gate of the MOSFET when the SMC is in action

The application of switching pulses charge the energy storage devices and the stored energy is discharged to the load and this operation happens during every switching cycle. This causes a change in the voltage drop across the inductors and capacitors and the voltage across the inductor 1 is represented in figure 25(a). Since the voltage is boosted in cascade the voltage across the inductor L_2 is much more than that across inductor L_1. The voltage across the inductor L_2 for the same duty cycle is represented in figure 25(b).

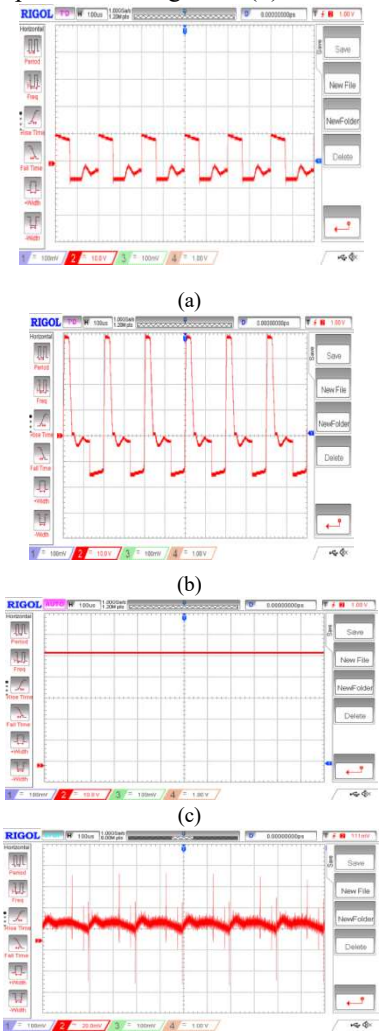

(a)

(b)

(c)

(d)

Figure. 25 (a) The voltage across the inductor L1, (b) The voltage across the inductor L2, (c) The DC output voltage of 54 V with the system under open-loop condition, (d) The ripple in the DC voltage output of the QBC

The topology of the QBC is built around two inductors and two capacitors and a common power electronic switch. However, the complete QBC can be treated as the series

combination or cascading of two generic boost converters. The overall order of the system is four. The steady-state DC voltage of the QBC with any duty cycle is almost steady, stable and is free from ripple as shown in figure 25(c). However, with the inclusion of the closed-loop controller like the SMC and because of the inherent switching operation happening in the circuit there are little ripple notices. The ripple content of the output of the QBC is represented in the figure 25(d) and the peak value of the ripple noticed is just 20 mV peak to peak.

V. Conclusion

The Quadratic Boost Converter is emerging as an important entity in the development of the microgrid. A detailed analysis of the quadratic boost converter in the light of the state-space averaging method has been carried out. In consideration of the non-linearity exhibited an SMC has been proposed. The stability analysis of the SMC for the QBC has been carried out by the Lyapunov stability analysis method. The circuit model realized in MATLAB SIMULINK and the experimental prototype both included an SMC and the proposed control scheme has shown greater performance as compared to the PI controller and the Fuzzy Logic Controller.

References

[1] VitorFernãoPires, Daniel Foito, Armando Cordeiro. A DC–DC Converter With Quadratic Gain and Bidirectional Capability for Batteries/Supercapacitors. IEEE Transactions on Industry Applications 2018;54(1);274 - 285.

[2] L.H.S.C. Barreto, E.A.A. Coelho, V.J. Farias, J.C. de Oliveira, L.C. de Freitas, Jr. Joao B. A quasi-resonant quadratic boost converter using a single resonant network. IEEE Transactions on Industrial Electronics 2005;52(5);552 - 557.

[3] Yijie Wang, YupingQiu,QingBian, Yueshi Guan, DianguoXu. A Single Switch Quadratic Boost High Step Up DC–DC Converter. IEEE Transactions on Industrial Electronics 2019;66(6);4387 - 4397.

[4] Neng Zhang, Guidong Zhang, KhayWai See, Bo Zhang. A Single-Switch Quadratic Buck–Boost Converter With Continuous Input Port Current and Continuous Output Port Current.IEEE Transactions on Power Electronics 2018;33(5);4157 - 4166.

[5] Olive Ray, Santanu Mishra. Boost-Derived Hybrid Converter With Simultaneous DC and AC Outputs. IEEE Transactions on Industry Applications 2014;50(2);1082 - 1093.

[6] J. Leyva-Ramos, R. Mota-Varona, M. G. Ortiz-Lopez, L. H. Diaz-Saldierna, D. Langarica-Cordoba.Control Strategy of a Quadratic Boost Converter With Voltage Multiplier Cell for High-Voltage Gain.IEEE Journal of Emerging and Selected Topics in Power Electronics 2017;5(4);1761 - 1770.

[7] SatyajitHemantChincholkar, Chok-You Chan. Design of Fixed-Frequency Pulsewidth-Modulation-Based Sliding-Mode Controllers for the Quadratic Boost Converter.IEEE Transactions on Circuits and Systems II: Express Briefs 2017;64(1);51 - 55.

[8] Xueshan Liu, Xuewen Li, Qun Zhou, JianpingXu. Flicker-Free Single-Switch Quadratic Boost LED Driver Compatible With Electronic Transformers. IEEE Transactions on Industrial Electronics 2019;66(5);3458 - 3467.

[9] VitorFernãoPires, Armando Cordeiro, Daniel Foito, Jose Fernando Silva. High Step-Up DC–DC Converter for Fuel Cell Vehicles Based on Merged Quadratic Boost–Ćuk. IEEE Transactions on Vehicular Technology 2019';68(8);7521 - 7530.

[10] NengZhang ; Danny Sutanto ; Kashem M. Muttaqi ; Bo Zhang ; DongyuanQiu. High-voltage-gain quadratic boost converter with voltage multiplier. IET Power Electronics 2015;8(12);2511 - 2519.

[11] Francesco Alonge, Roberto Rabbeni, Marcello Pucci, Gianpaolo Vitale. Identification and Robust Control of a Quadratic DC/DC Boost Converter by Hammerstein Model.IEEE Transactions on Industry Applications 2015;51(5); 3975 - 3985.

[12] Mustafa A. Al-Saffar, Esam H. Ismail, Ahmad J. Sabzali. Integrated Buck–Boost–Quadratic Buck PFC Rectifier for Universal Input Applications.IEEE Transactions on Power Electronics 2009;24(12);2886 - 2896.

[13] Oswaldo López-Santos, Luis Martínez-Salamero, GermainGarcía, Hugo Valderrama-Bla. Efficiency analysis of a sliding-mode controlled quadratic boost converter.IET Power Electronics 2013;6(2);364 - 373.

[14] Mengting Zhang, Xiuliang Li, Jia Liu, HongyeSu. Dual-mode LQR-feedforward optimal control for non-minimum phase boost converter.IET Power Electronics 2017;10(1);92 - 102.

[15] WentaoJiang ;SatyajitHemantChincholkar ; Chok-You Chan. Modified voltage-mode controller for the quadratic boost converter with improved output performance. IET Power Electronics;11(14);;2222 - 2231.

[16] Zhengge Chen, Ping Yang, Guohua Zhou, JianpingXu, Zhangyong Chen. Variable Duty Cycle Control for Quadratic Boost PFC Converter. IEEE Transactions on Industrial Electronics 2016;63(7);4222 - 4232.

[17] J.a. Morales-Saldana ; R. Galarza-Quirino ; J. Leyva-Ramos ; E.e. Carbajal-Gutierrez ; M.g. Ortiz-Lopez. Multiloop controller design for a quadratic boost converter.IET Electric Power Applications 2007;1(3);362 - 367.

[18] Saman A. Gorji, Ali Mostaan, Hung Tran My, MehranEktesabi. Non-isolated buck–boost dc–dc converter with quadratic voltage gain ratio.IET Power Electronics 2019;12(6);1425 - 1433.

[19] Jesus E. Valdez-Resendiz, Julio C. Rosas-Caro, Jonathan C. Mayo-Maldonado, Armando. Quadratic boost converter based on stackable switching stages. IET Power Electronics 2018;11(8);1373 - 1381.\

[20] Yuan-mao Ye, KaWai Eric Cheng. Quadratic boost converter with low buffer capacitor stress. IET Power Electronics 2014; 7(5);1162 - 1170.

[21] Sin-Woo Lee, Hyun-Lark Do. Quadratic Boost DC–DC Converter With High Voltage Gain and Reduced Voltage Stresses.IEEE Transactions on Power Electronics 2019;34(3);2397 - 2404.

[22] Anish Ahmad, Vinod Kumar Bussa,Rajeev Kumar Singh, RanjitMahanty. Quadratic boost derived hybrid multi-output converter. IET Power Electronics 2017;10(15);2042 - 2054.

[23] Julio C. Rosas-Caro, Jesus E. Valdez-Resendiz, Jonathan C. Mayo-Maldonado, AvelinaAlejo-Reyes, Antonio Valderrabano-Gonzalez. Quadratic buck–boost converter with positive output voltage and minimum ripple point design.IET Power Electronics 2018;11(7);1306 - 1313.

[24] Jonathan C. Mayo-Maldonado, Jesus E. Valdez-Resendiz, Pedro M. Garcia-Vite, Julio C. Rosas-Caro, M. del Rosario Rivera-Espinosa, Antonio Valderrabano-Gonzalez Quadratic Buck–Boost Converter With Zero Output Voltage Ripple at a Selectable Operating Point.IEEE Transactions on Industry Applications 2019;55(3);2813 - 2822.

[25] António Manuel Santos Spencer Andrade, MárioLȩcio da Silva Martins. Quadratic-Boost With Stacked Zeta Converter for High Voltage Gain Applications. IEEE Journal of Emerging and Selected Topics in Power Electronics 2017;5(4);1787 - 1796.

[26] Marcelo FlavioGuepfrih, GierriWaltrich, TellesBrunelliLazzarin. Quadratic-boost-double-flyback converter. IET Power Electronics 2019;12(12);3166 - 3177.

[27] MangaiyarkarasiPalaveashem, KavithaAnbukumar. Reduced order linear quadratic regulator controller for voltage multiplier cells integrated boost converter. IET Circuits, Devices & Systems 2016;10(6);536 - 548.

[28] Oswaldo Lopez-Santos, Luis Martinez-Salamero, Germain Garcia, Hugo Valderrama-Blavi, Tomás Sierra-Polanco. Robust Sliding-Mode Control Design for a Voltage Regulated Quadratic Boost Converter.IEEE Transactions on Power Electronics 2015;30(4); 2313 - 2327.

[29] Oswaldo Lopez-Santos, Luis Martinez-Salamero, Germain Garcia, Hugo Valderram. Steady-State Analysis of Inductor Conduction Modes in the Quadratic Boost Converter. IEEE Transactions on Power Electronics 2017;32(3);2253 - 2264.

[30] J. Leyva-Ramos, M.G. Ortiz-Lopez, L.H. Diaz-Saldierna, J.A. Morales-Saldana. Switching regulator using a quadratic boost converter for wide DC conversion ratios.IET Power Electronics 2009;2(5);605 - 613.